Hydrothermal Synthesis of LaCoO₃ Perovskite Catalyst and Its Application for the Degradation of Phenol under Visible Light

Niu, Ziyan; Guo, Shilong; Li, Jinchun; Qiao, Fengrui; Wang, Jin; Yang, Caifeng; Gao, Chuangji; Zhou, Jialiang; Liu, Zhenmin; Sun, Hongyan; Wang, Xiaoxiao*+

College of Chemical Engineering and Technology, Shanxi Key Laboratory of High-Value Utilization of Coal Gangue, Taiyuan University of Science and Technology, Taiyuan, P.R. CHINA

Wei, Xianxian; Guo, Shaoqing*+

School of Environment and Resources, Taiyuan University of Science and Technology, Taiyuan, P.R. CHINA

Xue, Yongbing

Instrumental Analysis Center, Taiyuan University of Science and Technology, Taiyuan, P.R., CHINA

ABSTRACT: *In this study, a series of LaCoO₃ perovskite catalysts with varying calcination temperatures were synthesized hydrothermally, and their structure, morphology, and optical properties were investigated using X-Ray powder Diffraction (XRD), Scanning Electron Microscopy (SEM), Fourier transform infrared spectroscopy (FT-IR), X-ray electron spectroscopy analysis (XPS), Magnetic Property Measurement System (MPMS), and other characterization techniques. Using phenol as the target degradation product, the photocatalytic degradation reaction was carried out in the presence of visible light. In addition, the photocatalytic mechanism of LaCoO₃ perovskite was also discussed. The experimental results showed that the LaCoO₃ perovskite catalyst has been prepared with good crystallization. The particle size of the catalysts ranged from 10 to 40 nm, and the specific surface area decreased with calcination depth. Moreover, all the LaCoO₃ catalysts showed strong paramagnetism, and the particles were regularly agglomerated under the action of magnetic force. LaCoO₃ catalyst (the calcination temperature of 750 °C) exhibited high photocatalytic activity. In addition, the study of photocatalytic mechanisms revealed three degradation pathways for degrading phenol into inorganic small molecules such as CO_2 and H_2O via highly active HO•, HO_2•, and h^+ radicals.*

KEYWORDS: *Perovskite; LaCoO₃; Catalyst; Photocatalysis; Phenol.*

INTRODUCTION

Phenol, as an essential chemical material, is widely utilized in different industries of leather, petroleum, chemical and pharmaceutical [1-2]. And approximately 700 million tons of phenol is produced every year. Phenol is one of the most toxic organic pollutants and has been listed in the US EPA priority list of hazardous substances discarded into the aquatic environment [3-6]. The discharge of phenolic wastewater not only limits plant growth, but also pollutes the ecological environment, and further affects the survival and health of the human [7-10]. Therefore, an efficient treatment is urgently needed for the degradation of phenolic wastewater.

At present, there are many methods for the degradation of phenol in the organic wastewater [11-18]. *Leitao et al.* found that the halotolerant strain penicillium chrysogenum had a good degradation effect on phenol [12]. *Li et al.* studied the degradation of phenol with macroporous resin and provided theoretical reference for the practical application of phenolic wastewater treatment [13]. *Luo et al.* degraded phenol using the diaphragm electrolysis device. Also the phenol removal rate could reach 100% after 40 min under the optimal conditions [14]. Compared with the above methods, photocatalytic degradation has become a preferred method for the degradation of phenol due to its many advantages, such as rapid degradation rate, low cost, no secondary pollution and strong oxidation capacity. However the conventional photocatalysts such as TiO_2 just could be stimulated under UV light and only used about 4% of the solar energy [19-21]. Therefore, it is necessary to research and develop visible-light-induced photocatalysts for the degradation of phenol.

Perovskite oxide semiconductors (ABO_3) have been demonstrated as promising photocatalysts due to their strong solar energy (visible light) absorption and high quantum efficiency [22]. The lanthanum (La) based materials have higher carbonaceous oxidation activity. The cobalt (Co) contained perovskite exhibits better catalytic activity due to its high electrical and ionic conductivities and its excellent electrochemical properties [23]. Hence, $LaCoO_3$ perovskite catalysts have aroused considerable attention, and are considered as attractive and efficient visible-light-induced photocatalyst for the removal of organic pollutants in water due to the advantages of stability, low cost, non-toxicity, and environmental friendliness.

Recently, there were many studies about the photocatalytic activity of $LaCoO_3$ perovskite catalyt [24-32]. *Sun et al* reported that the photocatalytic activity of $LaCoO_3$ have associated with the reducibility of Co^{3+} to some extent, and $LaCoO_3$ could be reused in recycle dye degradation when the calcination temperature was 800 °C [24]. Jung and co-workers discovered that the $LaCoO_3$ catalyst prepared using microwave-assisted method showed the high activity in the decomposition of methyl orange [25]. *Gao et al* prepared perovskite-type $LaCoO_3$ catalyst by hydrothermal method and studied its photocatalytic activity for the degradation of semi-coking waste water. The optimum reaction conditions were the amount of H_2O_2 was 3 mL, the mass of the catalyst was 0.2 g, pH was 4 and the reaction temperature was 25 °C. The COD removal rate of semi-coking waste water reached 72.7% under the optimum reaction conditions [26]. *Li et al* studied the influencing factors for the degradation of malachite green with $LaCoO_3$ as catalyst through changing the reaction time, the amount of catalyst, the initial concentration of raw materials and the pH of the solution. And the results showed that the photocatalytic activity of $LaCoO_3$ was high and the degradation rate of malachite green was up to 90.1% with 0.15 g catalyst in 100 mL, 10 mg/L malachite green degradation for 2 h [27]. From the above reaction results, it can be found that $LaCoO_3$ perovskite catalyst have indeed application in the photocatalytic degradation. However, there are few reports about the research of $LaCoO_3$ on its photocatalytic activity for the degradation of phenol under visible light.

In this study, a series of $LaCoO_3$ perovskite catalysts were synthesized with different calcination temperature by hydrothermal method and the physicochemical properties of synthesized samples were characterized by XRD, SEM, TEM, FT-IR, N_2 adsorption-desorption, XPS and so on. Furthermore, the photocatalytic degradation of phenol was also studied under visible light. Moreover, a possible photocatalytic mechanism was proposed.

EXPERIMENATAL SECTION
Materials

Lanthanum nitrate ($La(NO)_3 \cdot 6H_2O$, AR, 99%), cobalt nitrate($Co(NO)_3 \cdot 6H_2O$, AR, 99%), phenol(AR), citric acid (AR, ≥99.5), ammonia(AR, 25%), ethanol (AR, ≥99.7). The phenol solution was prepared into distilled water.

Catalyst preparation

A series of LaCoO$_3$ perovskite catalysts with varying calcination temperatures were synthesized by hydrothermal method [33] as displayed in Fig. 1. Firstly, La(NO$_3$)$_3$·6H$_2$O, Co(NO$_3$)$_2$·6H$_2$O and Citric acid were accurately weighed with composition of 1 La(NO$_3$)$_3$·6H$_2$O: 1 Co(NO$_3$)$_2$·6H$_2$O: 1 Citric acid, and dissolved in 80mL deionized water. Then, the solution was placed on a magnetic stirrer, and the pH value of the solution was adjusted to about 8.5 with ammonia water while stirring, so that the metal ions could completely precipitate. The mixture was poured into a teflon stainless steel reactor and reacted in an oven at 150 °C for 20h. Centrifuge was used to filter the supernatant, and the mixture was washed with deionized water and ethanol several times, respectively. The powder was dried in an oven at 120 °C, and after grinding, the powder was pre-burned for 2 hours at 550 °C, 650 °C, 750 °C and 850 °C respectively in a box-type resistance furnace. Finally, the sample of powder LaCoO$_3$ was obtained. The synthesized LaCoO$_3$ catalyst is named LCO-550, LCO-650, LCO-750 and LCO-850 respectively according to different calcination temperature.

Catalyst characterization

X-ray powder diffraction (XRD) analysis was carried out on D/max-2500 X-ray diffractometer of Rigaku company in Japan. Diffraction patterns were recorded with Cu Ka radiation at 40 kV and 100 mA in the scan range between 5° and 90° to identify the phase structure of the sample. The data was automatically collected by the computer.

Scanning electron microscopy (SEM) was performed with a LEO-435VP scanning electron microscopy operated at 20 kV and 50 PA equipped with energy-dispersive spectrometer (EDS) was used to examine the properties of prepared samples, including the surface morphology, the elements and the composition of the prepared samples.

High-resolution transmission electron microscopy (TEM) was carried out to further characterize the microstructure of the samples. The samples were prepared as follows: a small amount of the examined materials was carried out in 1.25 cm^3 of ethanol. A few drops from this suspension were deposited and dried onto the surface of the grid (CF 200 Cu TEM grid).

Fourier Transform InfraRed (FT-IR) spectroscopy spectra of the samples were obtained using a Nicolet 380 FT-IR spectrometer. Scan from 4000cm^{-1} to 400cm^{-1} with a resolution of 4.0 cm^{-1}.

The textural properties of the samples were derived from N$_2$ adsorption-desorption measurement on Micromeritics Tristar 3000. In each case, the sample was outgassed under vacuum at 300 °C for 3 h before N$_2$ adsorption. The specific surface area was calculated according to BET method and the volume of porous was obtained by t-plot analysis of the adsorption isotherm.

The X-ray electron spectroscopy analysis (XPS) spectra were measured by using a Kratos XSAM800 fitted with an Al Kα source (1486.6 eV) with two ultra-high-vacuum (UHV) chambers. The binding energy was referenced to the C1s peak (284.8 eV) to account for charging effects. The areas of the peaks were computed after fitting of the experimental spectra to Gaussian/Lorentzian curves and removal of the background (Shirley function).

Magnetic Property Measurement System (MPMS) was equipped with a superconducting magnet and liquid ammonia temperature control system, which provides a high magnetic field and extremely low-temperature measurement environment. The high sensitivity of MPMS comes from the equipment core SQUID, which is used to detect magnetic signals. The whole measurement process (including data acquisition, processing, and analysis) was highly automated. In this magnetic measurement experiment, the magnetic properties of the obtained powder were tested directly without pre-treatment.

H$_2$-temperature programmed reduction (H$_2$-TPR) were carried out in a Canta Quantachrome automatic temperature programmed chemisorption instrument ChemBET to pretreat about 0.1 g of sample at 300 °C with He gas with flow rate of 30 ml/min for 1 hour, then reduce to room temperature, change the gas to H$_2$/He mixture, wait for 30 min, blow away the He gas existing in the instrument, and after the baseline is stable, raise the temperature to 950 °C and 10 °C per minute to analyze the recorded signal.

Photocatalytic activity tests

All as-prepared LaCoO$_3$ catalysts were evaluated for the degradation of phenol under visible light using a PLS-SXE300 xenon lamp as the light source. 250 mL
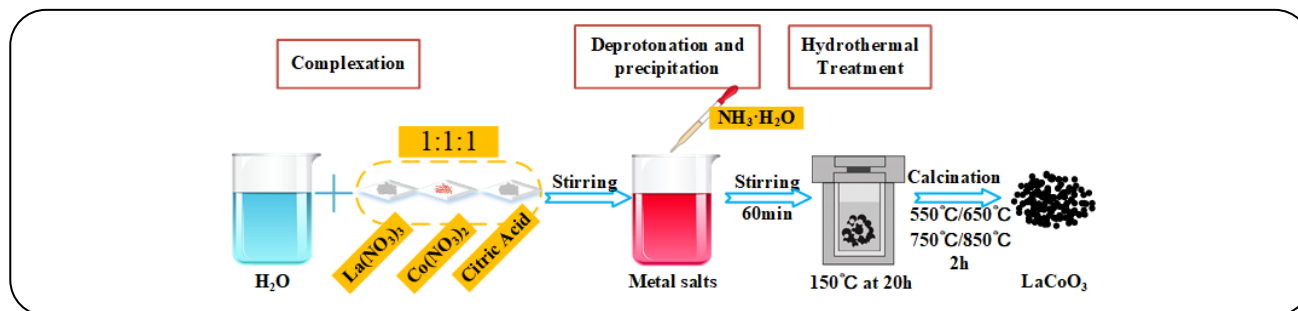
Fig. 1: Schematic diagram for the synthesis of LaCoO$_3$ perovskite catalyst.

jacketed beaker was used as a reactor, and the reaction temperature was holed at 20 ℃ by circulating water. After that, 100 mg LaCoO$_3$ catalysts were magnetically dispersed in 100 mL, 10 mg/L phenol solution. Prior to light irradiation, the dispersion was firstly stirred for 40 min in the dark to reach the adsorption-desorption equilibrium between phenol and the catalyst surface. After that 2 mL of the specified dispersions were extracted at given time intervals (the irradiation time intervals of 30 min). The specified dispersions were dropped in a cuvette to record the UV-Vis absorption spectra at 270 nm by a UV-2550 spectrophotometer to monitor the concentrations of phenol. The degradation experiments of phenol were also carried out in the absence of visible light and without the addition of the photocatalyst under the same conditions.

In general, the photocatalytic degradation efficiency can be calculated by the formula $D(\%)=(C_0-C)/C_0\times100\%$ calculation. The initial concentration (C_0) of phenol and the concentration (C) of phenol after degradation for a certain time was measured by UV-Vis spectrophotometer to calculate the degradation rate.

RESULTS AND DISCUSSION
Structure characterization
XRD

XRD technology was used to analyze the phase and composition of the prepared sample (Fig. 2). Comparing the obtained LaCoO$_3$ spectrum with the standard spectrum [34], it can be seen that the characteristic diffraction peaks of LaCoO$_3$ (2θ=23.38°, 32.81°, 40.73°, 47.74°, 53.65°, 59.00°, 69.15° and 78.95°) were observed for all synthesized samples, which was attributed to (012), (110), (202), (024), (116), (214), (220) and (134) lattice planes (JPCDS No.48-0123), respectively. Meanwhile, it should be noted that there was no other heterophase existed

in Fig. 2 and the diffraction peak intensity of LaCoO$_3$ increased first (from 550 °C to 750 °C) and then decreased (from 750 °C to 850 °C) with the increase of calcination temperature. It has been reported that the perovskite-like material only formed at an appropriate temperature, high calcination temperature could interfere with the crystal formation of perovskite catalyst because of sintering and result in crystal growth, and will further lead to the decrement of surface area [35-36]. There, the best calcinations temperature for the synthesis of LaCoO$_3$ perovskite catalyst was 750 °C.

SEM

The morphologies and microstructures of the as-prepared LaCoO$_3$ samples were investigated by SEM, and simultaneously introduced the SEM-EDX spectrum to study the elements distribution of LaCoO$_3$. As shown in Fig.3, the particles of samples uniformly distributed and the particle size was within the range of 20 nm to 40 nm. And the average particle size increased gradually with increasing the calcination temperature.

In addition, EDS analysis was also used to further study the elemental composition of LaCoO$_3$ catalyst. The spectral peak in the EDS represented the elements in the sample, and the atomic percentage of each element was obtained by region scanning. And the result of the analysis is shown in Table 1, It can be seen from Table 1 that the proportion of each element was basically La:Co:O=1:1:3 in the sample, and the content of O element was slightly higher, and the analysis result was approximately consistent with the structural proportion of perovskite ABO$_3$. At the same time, no other additional peaks appeared in the EDX spectrum, indicating the purity of the prepared LaCoO$_3$ catalyst.

Table 1: Atomic percentage content of LaCoO₃ catalyst synthesized.

At%	LCO-550	LCO-650	LCO-750	LCO-850
La	14.2%	11.4%	10.2%	14.4%
Co	12.1%	12.3%	14.4%	14.0%
O	63.9%	66.5%	49.8%	58.2%
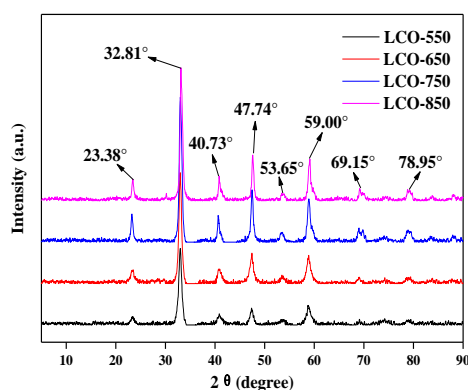
Fig. 2: XRD patterns of LaCoO₃ catalysts at different calcination temperatures.

TEM

Fig.4 shows the TEM images of LCO-750 catalyst. As shown in Fig.4, the particle size of $LaCoO_3$ was between 10 nm to 40 nm, and most of the grain boundaries were clear, but there was a certain degree of agglomeration between the particles. Regular and complete lattice fringes can be seen from Fig.4c, which showed that LCO-750 had a good degree of crystallization. After measurement, the crystal plane spacing corresponding to lattice fringes were 0.269, 0.272 and 0.383nm, which corresponded to (104), (110), and (012) crystal planes of $LaCoO_3$ respectively. From here we can see that the above results were consistent with the results of XRD analysis.

FT-IR

FT-IR was performed to confirm the composition and structure of the as-prepared $LaCoO_3$. Fig.5 shows the IR spectra of $LaCoO_3$ prepared at different calcination temperatures, and the attribution of their main absorption peaks is shown in Table 2. It can be seen that the absorption peak with wave numbers of about $421cm^{-1}$ and $556cm^{-1}$ belonged to the bending vibration peak of O-Co-O and the stretching vibration

peak of Co-O, respectively [37]. There was a strong peak with a wave number of $600\sim611cm^{-1}$, which is attributed to the stretching vibration peak of Co-O in the pure calcium titanium mineral phase [38]. Therefore, it can be easily seen that all characteristic peaks of $LaCoO_3$ were observed and no new chemical bonds or solvent residue absorption peaks were detected, which were consistent with the XRD analysis results.

N₂ adsorption-desorption

Table 3 presented the pore structure parameters of as-prepared $LaCoO_3$ catalysts. It can be seen that the surface area of $LaCoO_3$ catalyst decreased with the increase of calcination temperature, which found further evidence to support the results of XRD analysis. In addition, Table 3 showed that the surface area of all catalysts were small, which may be because citric acid was not a good complexing agent for preparing perovskite metal oxides with high surface area. It suddenly released a lot of energy during calcination, resulting in pore collapse [39].

The N_2 adsorption-desorption isotherms of as-prepared $LaCoO_3$ catalysts were shown in Fig.6. According to the IUPAC classification, all catalysts showed type IV isotherms and had H3 hysteresis loops. A hysteresis between adsorption and desorption branches was observed at medium relative pressure $(0.9-1.0)$ for all the samples, which demonstrated that the hysteresis loop did not show adsorption saturation in the region of higher relative pressure. And the pore diameters of all the samples were between 2-50 nm, indicating that the pore diameters were mesoporous with flake particle structure or slit structure. In addition, the adsorption volume of the four catalysts decreased in the following order: LCO-550 > LCO-650 > LCO-750 > LCO-850, indicating that the surface area of them decreased gradually, which were in good agreement with the results of Table 3.
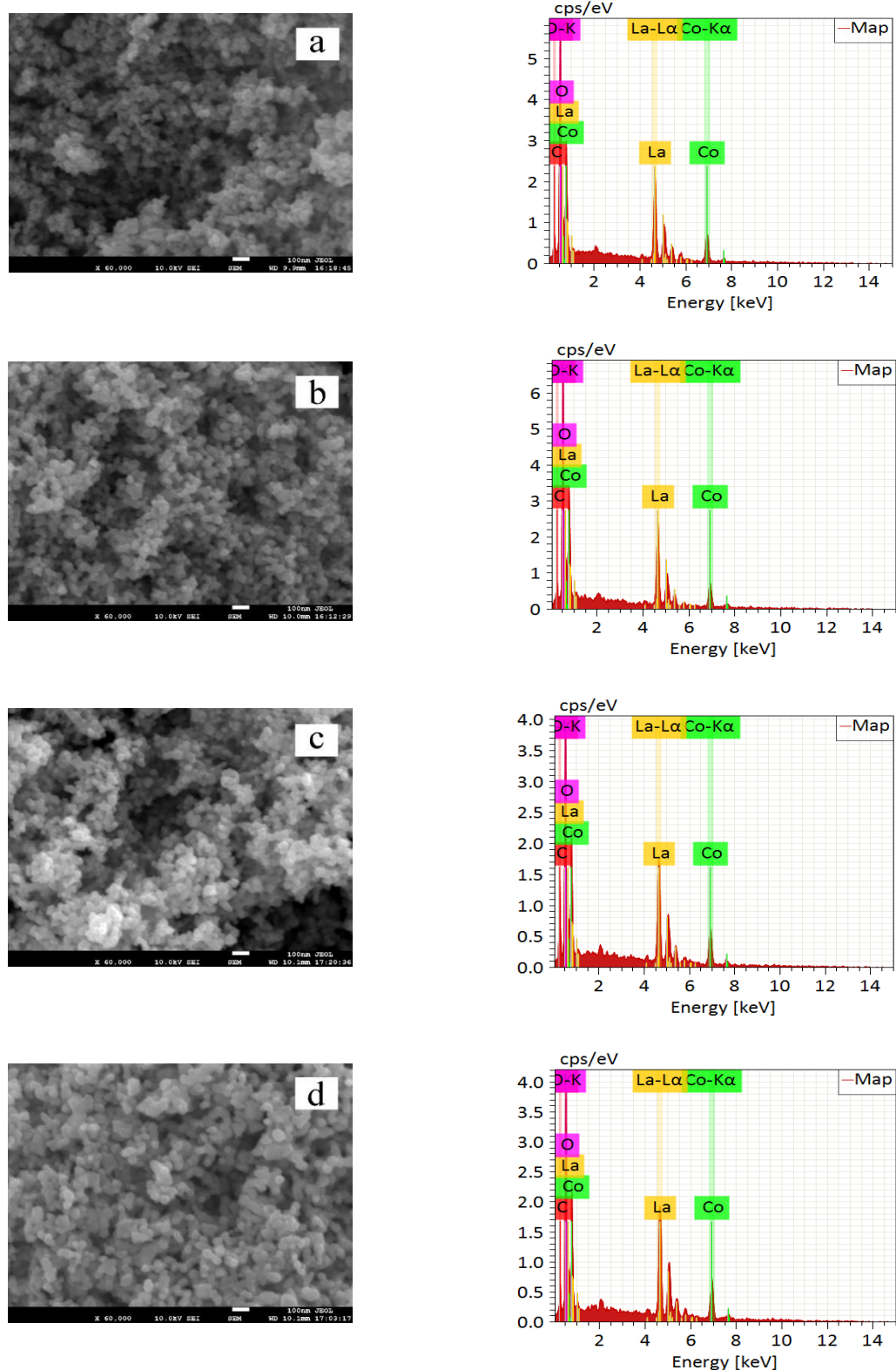
Fig. 3: SEM images and EDS spectra of LaCoO₃ catalyst at different calcination temperatures. (a) LCO-550, (b) LCO-650, (c) LCO-750, (d) LCO-850

Table 2: FT-IR attribution analysis of as-prepared LaCoO₃ catalysts.

Wavenumber/cm⁻¹				Ascription
LCO-550	LCO-650	LCO-750	LCO-850	
428	421	429	418	O-Co-O
555、603	558、602	555、611	556、600	Co-O

Table 3:

Catalyst	Surface Area/m²·g⁻¹	Pore Volume/cm³·g⁻¹	Pore Size/nm
LCO-550	30.72	0.170	22.14
LCO-650	22.23	0.110	19.84
LCO-750	17.20	0.064	15.05
LCO-850	15.36	0.069	17.86
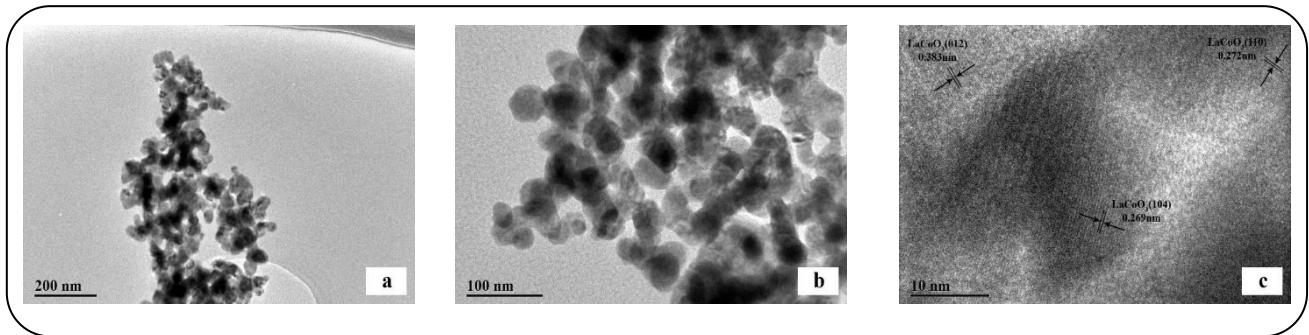
Fig.4: TEM images of LCO-750 catalyst.
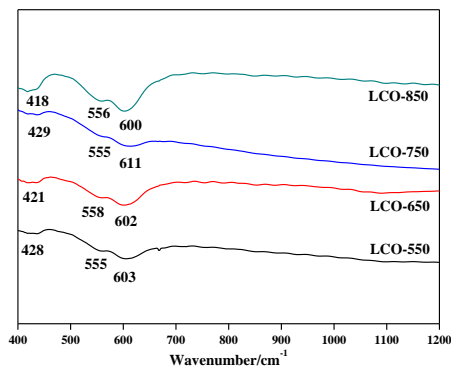
Fig.5: FT-IR spectrum of as-prepared LaCoO₃ catalyst.
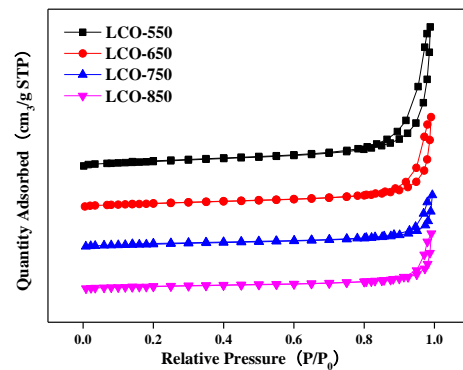
Fig.6: N₂ adsorption-desorption isotherms of as-prepared LaCoO₃ catalysts.

XPS

XPS technique was carried out to analyze the surface chemical composition and element chemical state of as-prepared samples. Fig.7 shows the data obtained from XPS spectra by peak splitting fitting for catalysts at different calcination temperatures. The elemental composition and valence state of LaCoO₃ were also studied by XPS. The full spectrum of all the samples was compared in Fig.7a showed that as-prepared LaCoO₃ catalysts contained La, Co, O, and C, which was consistent
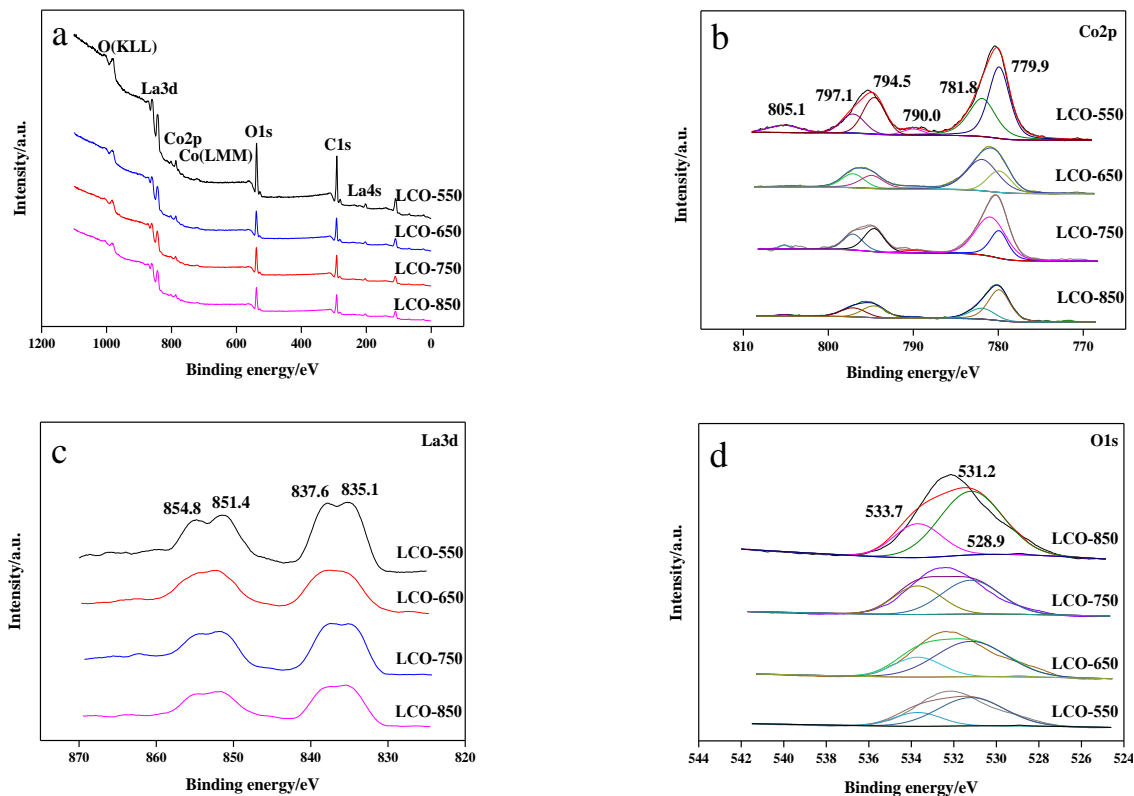
Fig.7: XPS analysis energy spectrum of as-prepared LaCoO₃ catalysts.

with the results of EDS spectrum analysis. As shown in Fig.7b (the XPS spectra of Co2p), four peaks at 779.9, 781.8, 794.5 and 797.1eV can be fitted and attributed to Co^{3+} and Co^{2+} species, respectively. The peak at 790.0eV was the satellite peak of Co^{2+} species. The peak at 805.1eV was attributed to the satellite peak of Co species in Co_3O_4 [40-41]. Fig.7c (the XPS spectra of La3d) showed that the peaks of La3d5/2 and La3d3/2 were split into two components by about 4eV, which was attributed to the accompanying ionization process of electron transfer from oxygen valence band to empty La4f orbit [42]. It can be seen from Fig.7d (the XPS spectrua of O1s) that three peaks at 528.9, 531.2 and 533.7eV could be fitted, which were attributed to lattice oxygen, oxygen on oxygen vacancy and surface oxygen, respectively. In addition, from the XPS spectrum of La, it was indicated that all La ions existed in the form of La^{3+} because La had a stable oxidation state and did not participate in the redox reaction as an active site [43].

MPMS

Fig.8 showed the magnetic properties of as-prepared LaCoO₃ catalysts. Compared with C and O elements,

La and Co elements were magnetic metal elements, and their M-H curves showed very strong linear characteristics [44-46]. As shown in Fig.8, the paramagnetism of all the samples decreased in the order of LCO-750 > LCO-850 > LCO-650 > LCO-550 under the same magnetic field intensity, which indicated that LaCoO₃ catalyst increased in nonlinear with the increase of calcination temperature. In addition, combining SEM images and MPMS characterization, we found that the smaller the particle size of LaCoO₃ catalyst was, the easier the catalyst was to be magnetized and then the catalyst showed high paramagnetism. In addition, Magnetism has a great impact on the recovery of catalysts, high paramagnetism of catalyst was helpful to reuse it.

H₂-TPR

H₂-TPR was used to detect the redox capacity of as-prepared LaCoO₃ catalysts, the H₂-TPR profiles of different catalysts samples were illustrated in Fig.9. As shown in Fig.9, there were two reduction stages in the range of 350-450 ℃ and 550-650 ℃, the reduction stage was attributed to the reduction of Co^{3+} to Co^{2+}
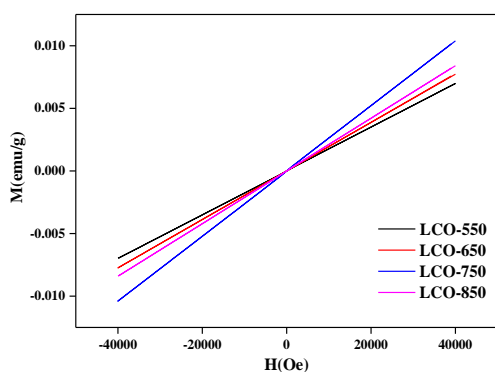
Fig.8: MPMS diagrams of as-prepared LaCoO₃ catalysts.

Fig.9: H₂-TPR profiles of as-prepared LaCoO₃ catalysts.

and the reduction of Co^{2+} to Co^0, respectively. It can be seen from Fig.9 that compared other catalysts, LCO-650 exhibited strong reduction with the lowest temperature (386 ºC), while LCO-750 showed high stability due to its highest temperature (640 ºC) [47-48]. And LCO-750 has larger peak area than other catalysts, which indicated that the amount of reactive oxygen species of LCO-750 were more than those of other catalysts, and then more hydrogen were involved in the reaction. In addition, through the previous SEM analysis, it was found that the particle size of the powder samples obtained at different calcination temperatures were almost the same and the distribution were relatively uniform. However, the XRD results showed that the crystallinity of LCO-750 was the largest. Therefore, we speculated that it may be due to the different crystallinity of different catalysts.

Photocatalytic performance

The degradation rate of as-prepared LaCoO₃ catalysts for phenol were shown in Fig.10. As the figure showed, the degradation rate of phenol for these catalysts first increased and then decreased with the calcination temperature. Compared with other catalysts, LCO-750 exhibited the best photocatalytic activity for phenol and the degradation rate of LCO-750 reached 52.56 % with 4 h reaction time. On the contrary, the degradation rate of LCO-850 was only 31.52 % with reaction time of 4 h. And the phenol degradation rates of LCO-550 and LCO-650 were 33.24 % and 48.93 %, respectively.

In addition, combining the characterization results of XRD and SEM, it was found that the particle size of LCO-550 and LCO-650 have little difference and the distribution of them were more uniform than that of LCO-
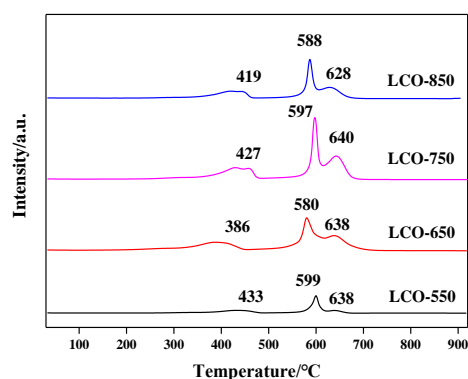
750 and LCO-850. However, XRD results showed that the crystallinity of LCO-650 was better than that of LCO-550, therefore LCO-650 exhibited better photocatalytic performance in comparison with LCO-550. When the calcination temperature reached 750 ºC, the crystallinity and particle size increased, the defects decreased, and then LCO-750 presented higher photocatalytic performance than other catalysts. From H₂-TPR analysis results, we knew that LCO-750 has a larger peak area than other catalysts, indicating that the number of reactive oxygen species participating in the reaction of LCO-750 was more than that of other catalysts in the process of the hydrogen reduction reaction, and then the stability was also better than that of other catalysts, which has a direct impact on the photocatalytic performance of the catalyst. Fig.10 showed that LCO-850 exhibited lower photocatalytic performance than other catalysts, it is possible that the surface area of LCO-850 was the smallest among all the catalysts.

Meanwhile, in order to verify whether phenol would degrade by itself under visible light irradiation, took 100 mL phenol solution and kept other conditions unchanged without catalyst at 300 W (λ≥400nm) under the irradiation of xenon lamp for 4 hours, took 2 mL of mixed solution from the system every 30min, measured its absorbance with UV-VIS spectrophotometer, calculated the concentration through the standard curve, and the degradation rate curve was showed in the Fig.10. It was calculated that the degradation rate of phenol under the condition of xenon lamp irradiation was 1.33%. As we can see, phenol did not have any self-degradation in the absence of photocatalyst, which suggested the high stability of phenol under the light illumination.
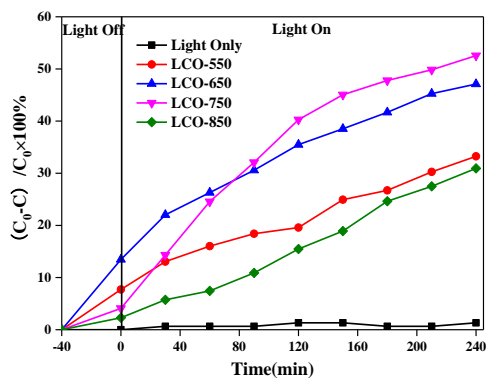
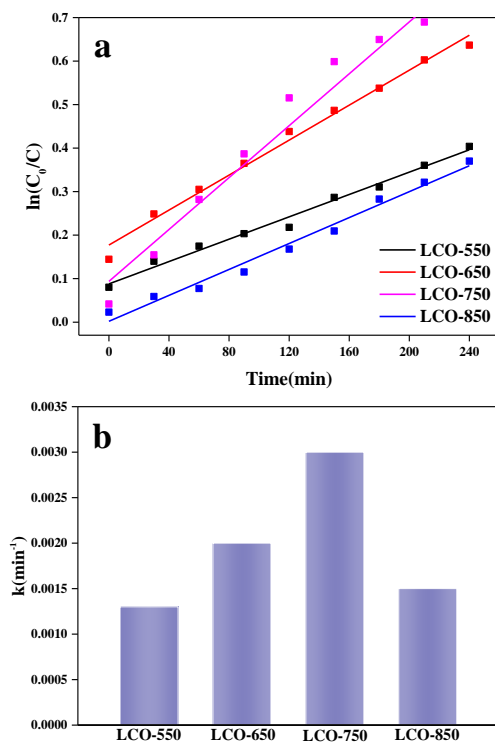**Fig.10: Degradation rate of as-prepared LaCoO₃ catalysts under different conditions.**

Fig. 11: The corresponding kinetic plots of phenol degradation over different catalyst.

To quantitatively compare photocatalytic degradation activity, the kinetic curves for degradation of phenol were obtained by a linear plot of $\ln(C_0/C)$ against degradation time. As can be seen, the kinetic curves can be fitted by a pseudo-first-order model as Eq.: $\ln(C_0/C)=kt$, where k, C_0 and C were the observed rate constant, phenol initial concentration and phenol concentration at time t,

respectively. Fig.11a displayed a linear relationship between $\ln(C_0/C)$ and t, which showed that the photodegradation reaction obeyed the pseudo-first-order kinetic. The corresponding observed rate constants for different products are shown in Fig.11b. Obviously, the k values of LCO-750 catalyst was higher than those of other catalysts. The k value of LCO-750 catalyst was the largest (0.003 min⁻¹), which was about 2.3, 1.5, 2.0 times of LCO-550 (0.0013 min⁻¹), LCO-650 (0.002 min⁻¹), and LCO-850 (0.0015 min⁻¹), respectively. Therefore, it was considered that LaCoO₃ catalyst synthesized by this method at 750 °C had better photocatalytic performance for phenol.

Catalyst reusability

It is widely known that the regeneration of the spent catalyst is one of the important factors to promote catalyst usability, therefore the photocatalytic activity of the spent catalyst was also investigated. We recovered the spent LCO-750 catalyst by centrifugation, the catalysts were placed in the beaker, and then absolute ethanol was added. After the ultrasound, the solutions were washed with absolute ethanol and deionized water several times, finally, the catalysts were put into the oven for drying and stored for studying the photocatalytic performance.

The phenol degradation rate of the spent LCO-750 catalyst 5 times was shown in Fig.12, as shown in Fig.12, the degradation rate still reached more than 40% after 5 times, which showed that the spent LCO-750 catalyst still had photocatalytic activity after repeated use. Therefore, it was considered that the LaCoO₃ catalyst had high reusability and stability.

Photocatalytic mechanism

From the above, we have known that perovskite photocatalyst LaCoO₃ showed high photocatalytic performance under visible light. When LaCoO₃ was irradiated by sunlight and absorbed photon energy (greater than the bandwidth), the electrons were excited to the conduction band in its internal low-energy region. After the transition, photogenerated electrons(e^-) were formed in the catalyst, while photogenerated holes(H^+) were left in the corresponding valence band, and then reacted with a small amount of water and oxygen molecules in the air to form active functional groups with strong oxidation ability on the surface of the catalyst. Some of the electrons would
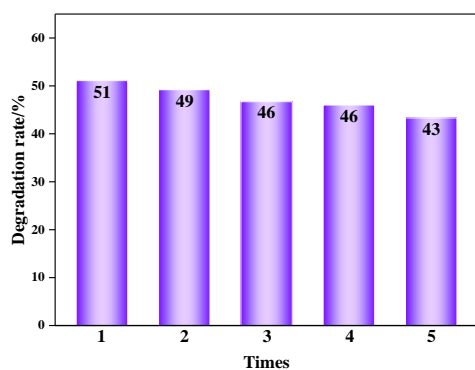
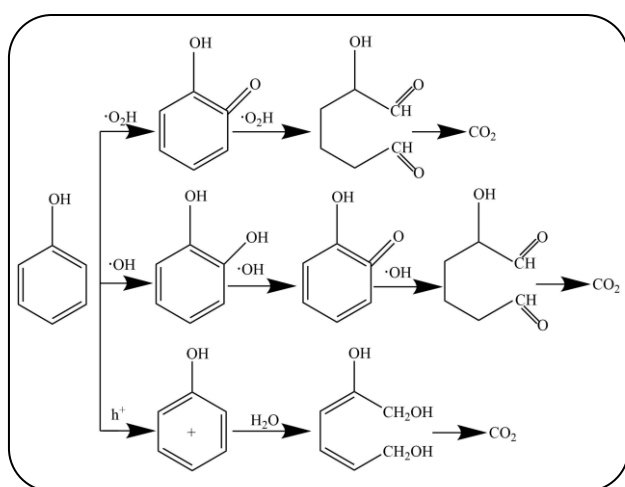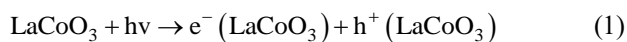*Fig.12: Reusability of the spent LCO-750 catalyst.*

Fig. 13: Degradation mechanism diagram of phenol.

also react with dissolved oxygen on the surface of the catalyst to form superoxide radical($\cdot O_2^-$), water molecules and photogenerated holes to form hydroxyl radical($\cdot OH$) [49-50].

The mechanism is as follows:

$$LaCoO_3 + hv \rightarrow e^- \left(LaCoO_3 \right) + h^+ \left(LaCoO_3 \right) \qquad (1)$$

$$h^+ + H_2O \rightarrow {}^\bullet OH + H^+ \qquad (2)$$

$$h^+ + OH^- \rightarrow {}^\bullet OH \qquad (3)$$

$$e^- + O_2 \rightarrow {}^\bullet O_2^- \qquad (4)$$

$$H_2O^+ + {}^\bullet O_2^- \rightarrow HO_2^\bullet + O^- \qquad (5)$$

The electron-hole pair converted the surface adsorbed oxygen into highly active free radicals such as HO• and HO₂• and then oxidized and reduced with the phenol

adsorbed on the catalyst surface together with the photogenerated holes also moved to the catalyst surface. The three degradation pathways would eventually degrade phenol into carbon dioxide, water, and some inorganic small molecules, playing the role of photocatalytic degradation of phenol pollutants. The photocatalytic degradation mechanism of phenol is shown in the Fig.13 below.

CONCLUSIONS

In this paper, A series of LaCoO₃ perovskite catalysts with different calcination temperatures were prepared by hydrothermal method and tested in the photocatalytic degradation reaction of phenol. Also, the physicochemical properties of as-prepared LaCoO₃ catalysts were characterized by XRD, SEM, TEM, FT-IR, XPS, MPMS, and so on. The XRD results showed that 750 °C was the optimum calcination temperature for the synthesis of LaCoO₃ perovskite catalyst. SEM images showed that the average particle size of the as-prepared increased gradually with increasing the calcination temperature. From N₂ adsorption-desorption characterization results, the surface area of all catalysts was small and the adsorption volume of the four catalysts decreased in the following order: LCO-550 > LCO-650 > LCO-750 > LCO-850. MPMS and H₂-TPR exhibited that LCO-750 has the highest paramagnetism and the largest peak area among all the catalysts, respectively.

Taking phenol as the target degradation product, the photocatalytic degradation reaction was carried out under visible light. The experimental results showed that exhibited higher photocatalytic activity than other catalysts, The degradation rate reached 52.56 percent after 4 hours of visible light irradiation at 20 ºC, and its rate constant k value was the highest (0.003), which was 2.3, 1.5, and 2 times higher than that prepared at calcination temperatures of 550 °C, 650 °C, and 850 °C, respectively. The analysis revealed that the average particle size of the catalyst calcined at 750 ℃ increased, the crystal crystallinity increased, defects were reduced, there were more active oxygen species involved in the reaction than other catalysts, and the stability was better than other catalysts, resulting in the best photocatalytic performance.

In addition, it was inferred from the study of photocatalytic mechanism that the electron-hole pair converted the adsorbed oxygen on the surface into highly

active free radicals such as HO• and HO$_2$• and then oxidized and reduced with the phenol adsorbed on the catalyst surface together with the photogenerated holes also moved to the catalyst surface. Under the action of visible light, the three degradation pathways would eventually degrade phenol into carbon dioxide, water, and some inorganic small molecules, playing the role of photocatalytic degradation of phenol pollutants.

REFERENCES

[1] Li H.Y., Li L.F., Xu W.F., Research Progress in Preparation of, *Chemical Engineering Design Communications*, **42(8)**: 48-49 (2016).

[2] Lyu C.Y., Zhang X.Z., Huang L., Yuan X.X., Xue C.C., Chen X., Widely Targeted Metabolomics Analysis Characterizes the Phenolic Compounds Profiles in Mung Bean Sprouts under Sucrose Treatment, *Food Chemistry*, **395(30)**: 133601-133612 (2022).

[3] Lin Y.S., Tang D.B., Liu X.M., Cheng J.R., Wang X.P., Guo D.L., Zou J.H., Yang H.G., Phenolic Profile and Antioxidant Activity of Longan Pulp of Different Cultivars from South China, *LWT - Food Science and Technology*, **165**: 113698-113707 (2022).

[4] Phshyev S., Demchuk Y., Polouzhyn I., Kochubei V., Obtaining and Use Adhesive Promoters to Bitumen from the Phenolic Fraction of Coal Tar, *International Journal of Adhesion and Adhesives*, **118**: 103191-103201 (2022).

[5] Özkan G., Özcan M.M., The Total Phenol, Flavonol Amounts and Antiradical Activity of some Oreganum Species, *Iranian Journal of Chemistry and Chemical Engineering (IJCCE)*, **37(4)**: 163-168 (2018).

[6] Zhang J., Zhang F., Lee Z.Z., Luo P.Y., Jeje A.A., Chen G., A Novel Botany Phenol Thinner Derived from Lignin and Its Application in Polymer Drilling Fluid, *Iranian Journal of Chemistry and Chemical Engineering (IJCCE)*, **37(2):** 241-246 (2018).

[7] Sheng Y., Harm of Phenol and Countermeasures, *Chemical Management*, **14**: 25-26 (2019).

[8] Liu J.Y., Zhang Y., Zhang L., Hua L., Zeng G.P., Yang C.Z., Research Progress in the Treatment Technologies of Industrial Wastewater Containing Phenol, *Industrial Water Treatment*, **38(10)**: 12-16 (2018).

[9] Zheng Q., Lee H.J., Lee J., Choi W.Y., Park N.B., Lee C.H., Electrochromic Titania Nanotube Arrays for the Enhanced Photocatalytic Degradation of Phenol and Pharmaceutical Compounds, *Chemical Engineering Journal*, **249(1)**: 285-292 (2014).

[10] Sheng X.B., Shen H.M., Sun Y.F., Zhao D.F., Study on Adsorption of Phenol by Polyferric Flocs, *Contemporary Chemical Industry*, **150(12)**: 10-13 (2021).

[11] Pradeep N.V., Anupama S., Navya K., Shalinl H.N., Idris M., Hampannavar U.S., Biological Removal of Phenol from Wastewaters: A Mini Review, *Applied Water Science*, **2:** 105-112 (2015).

[12] Leitao A.L., Duarte M.P., Oliveira J.S., Degradation of Phenol by A Halotolerant Strain of Penicillium Chrysogenum, *International Biodeterioration & Biodegradation*, **59**: 220-225 (2007).

[13] Li C., Zhong H., Zhou L., Zhao G., Study on Adsorption Characteristic of Macroporous Resin to Phenol in Wastewate, *The Canadian Journal of Chemical Engineerin*, **88**: 417-424 (2010).

[14] Luo H.J., Li C., Wu C., Wei Z., Dong X., Electrochemical Degradation of Phenol by in Situ Electro-Generated and Electro-Activated Hydrogen Peroxide using an Improved Gas Diffusion Cathode, *Electrochimica Acta*, **186**: 486-493 (2015).

[15] Zhang C., Cai X.L., Immobilization of Horseradish Peroxidase on Fe_3O_4/ Nanotubes Composites for Biocatalysis-Degradation of Phenol, *Composite Interfaces*, **26**: 379-396 (2019).

[16] Wang C., Zhao J., Chen C.M., Na P., Catalytic Activation of PS/PMS over Fe-Co Bimetallic Oxides for Phenol Oxidation under Alkaline Condition, *Applied Surface Science*, **562**: 150134-150143 (2021).

[17] Mohammad A., Khan M.E., Cho M.H., Yoon T., Adsorption Promoted Visible-Light-Induced Photocatalytic Degradation of Antibiotic Tetracycline by Tin Oxide/Cerium Oxide Nanocomposite, *Applied Surface Science*, **565:** 150337-150352 (2021).

[18] Nasiriyan M., Tabatabaee M., Mirhosaini S.A., Ehrampoush M.H., Lacunary Keggin-Type Hetero Polyoxometalate, $K_7PMo_2W_9O_{39}$, Supported on Nano ZnO as an Efficient Photocatalyst for Degradation of Phenol in Water Solution, *Iranian Journal of Chemistry and Chemical Engineering*, **40(5)**: 1414-1420 (2021).

[19] Wang Y.X., Yao Y.Z., Chen M.H., Preparation and Properties of TiO_2 Photocatalytic Materials, *Technology Innovation and Applicatio*n, **10**: 23-25 (2021).

[20] Ling H.J., Kim K., Liu Z.W., Shi J., Zhu X.J., Huang J., Photocatalytic Degradation of Phenol in Water on As-Prepared and Surface Modified TiO_2 Nanopariticles, *Catalysis Today*, **258**: 96-102 (2015).

[21] Wang X.Q., Xu H.L., Luo X.H., Li M., Dai M., Chen Q.H., Song H., Enhanced Photocatalytic Properties of CeO_2/TiO_2 Heterostructures for Phenol Degradation, *Colloid and Interface Science Communications*, **44**: 100476-100488 (2021).

[22] Zhang C.Q., Hen H.C., Wang N., Chen H.J., Kong D.T., Visible-light Sensitive $La_{1-x}Ba_xCoO_3$ Photocatalyst for Malachite Green Degradation, *Ceramics International,* **39**: 3685-3689 (2013).

[23] Hsieh T.H., Jhong F.H., Ray D.T., Fu Y.P., Electrical Properties of $(La_{0.9}Ca_{0.1})(Co_{1-x}Ni_x)O_{3-\delta}$ Cathode Materials for SOFCs, *Ceramics International,* **38**: 1785-1791 (2012).

[24] Sun M.M., Jiang Y.S., Li F.F., Xia M.S., Xue B., Liu D.R., Dye Degradation Activity and Stability of Perovskite-Type $LaCoO_{3-x}(x=0\sim0.075)$, *Materials Transactions,* **51**: 2208-2214 (2010).

[25] Jung W.Y., Hong S.S., Synthesis of $LaCoO_3$ Nanoparticles by Microwave Process and Their Photocatalytic Activity under Visible Light Irradiation, *Journal of Industrial and Engineering Chemistry,* **19**: 157-160 (2013).

[26] Gao W.W., Gong Y., Yan L., Chen B., Heterogeneous Fenton Reaction for Degradation of Semi-Coking Waste Water over Perovskite-Type $LaCoO_3$ Catalyst, *Industrial Catalysis*, **25(3)**: 71-75 (2017).

[27] Li J., Wei Z.X., Chen Z.M., Study on Photocatalytic Degradation of Malachite Green Dye by $LaCoO_3$, *Applied Chemical Industry,* **36**: 986-988 (2007).

[28] Wu W.W., Zhang H., Chang S.S., Gao J., Jia L.S., Study on the Antibacterial Performance of Perovskite $LaCoO_3$ under Visible Light Illumination, *Chemical Industry Times*, 23: 25-28 (2009).

[29] Chen H.L., Wei G.L., Liang X.L., Liu P., He H.P., Xi Y.F., Zhu J.X., The Distinct Effects of Substitution and Deposition of Ag in Perovskite $LaCoO_3$ on the Thermally Catalytic Oxidation of Toluene, *Applied Surface Science,* **489**: 905-912 (2019).

[30] Jayapandi S., Lakshmi D., Premkumar S., Packiyaraj P., Anitha K., Augmented Photocatalytic and Electrochemical Activities of Ag Tailored $LaCoO_3$ Perovskite Semiconductor, *Materials Letters,* **218**: 205-208 (2018).

[31] Tasleem S., Tahir M., Zakaria Z.Y., Z-scheme Ag-NPs-embedded $LaCoO_3$ Dispersed PCN Heterojunction with Higher Kinetic Rate for Stimulating Photocatalytic Solar H_2 Production, *Energy Conversion and Management,* **266**: 115786-115802 (2022).

[32] Luo J., Zhou X.S., Ning X.M., Zhan L., Ma L., Xu X.Y., Li S., Sun S.H., Utilization of $LaCoO_3$ as an Efficient Co-catalyst to Boost the Visible Light Photocatalytic Performance of g-C3N4, *Separation and Purification Technology,* **201**: 309-317 (2018).

[33] Zhang C.Q., "The Synthesis and Photocatalytic Properties of LaCoO₃-based Semiconductor Nanomaterials", M.S. Diss., University of Electronic Science and Technology of China (2012).

[34] Yang L.P., "Synthesis of Perovskite-type Composite Oxide and Study of its Photocatalytic Properties", M.S. Diss., Shanxi University (2010).

[35] Jia R.X., "Preparation and Characterization of Perovskite-Type Complex Oxides and Inquiry of its Activity", M.S. Diss., College of Chemical Engineering China University of Petroleum (East China) (2014).

[36] Zhu L.L., Lu G.Z., Wang Y.Q., Guo Y., Guo Y.L., Effects of Preparation Methods on the Catalytic Performance of $LaMn_{0.8}Mg_{0.2}O_3$ Perovskite for Methane Combustion, *Chinese Journal of Catalysis,* **31(8)**: 1006-1012 (2010).

[37] Tang C.W., Wang C.B., Chien S.H., Characterization of Cobalt Oxides Studied by FT-IR, Raman, TPR and TG-MS, *Thermochim. Acta,* **473**: 68-73 (2008).

[38] Kazuo N., "Infrared and Raman Spectra of Inorganic and Coordination Compounds. Part A: Therory and Applications in Inorganic Chemistry (Sixth Edition)", John Wiley & Sons, Inc., Hoboken, New Jersey, **419** (2009).

[39] Xiao X.Z., Lu G.Z., Mao D.S., Preparation of LaCoO₃ Catalyst and Its Catalytic Activity in Methane Catalytic Combustion Reaction, *Journal of Shanghai Institute of Applied Technology (Nat. Sci. Edition),* **14**: 1-5 (2014).

[40] Jia L.S., Qin Y.N., Ma Z., Ding T., Liang Z.C., XPS Study on Sulfurization Process of LaCoO₃ in the Presence of Oxygen, *Chinese Journal of Catalysis,* **25**: 19-22 (2004).

[41] Jin Z.H., Hu R.S., Wang H.Y., Hu J.A., Ren T., One-Step Impregnation Method to Prepare Direct Z-Scheme $LaCoO_3/g\text{-}C_3N_4$ Heterojunction Photocatalysts for Phenol Degradation under Visible Light, *Applied Surface Science,* **491(15)**: 432-442 (2019).

[42] Kucharczyk B., Tylus W., Effect of Pd or Ag Additive on the Activity and Stability Of Monolithic LaCoO₃ Perovskites for Catalytic Combustion of Methane, *Catalysis Today,* **90(1-2)**: 121-126 (2004).

[43] Dudric R., Vladescu A., Rednic V., Neumann M., Deac I.G., Tetean R., XPS Study on $La_{0.67}Ca_{0.33}Mn_{1-x}Co_xO_3$ Compounds, *Journal of Molecular Structure*, **1073(5)**: 66-70 (2014).

[44] Wang Y.G., "Hydrothermal Synthesis, Characterization and Properties of Perovskite Oxide Nanostructures", Ph.D. Diss., Zhejiang University (2009).

[45] Wang Y.G., Xu G., Ji X.P., Ren Z.H., Weng W.J., Du P.Y., Shen G., Han G.R., Room-temperature Ferromagnetism of Co-doped $Na_{0.5}Bi_{0.5}TiO_3$: Diluted Magnetic Ferroelectrics, *Journal of Alloys and Compounds,* **475(1-2)**: L25-L30 (2009).

[46] Wang Y.G., Xu G., Yang L.L., Ren Z.H., Wei X., Weng W.J., Du P.Y., Shen G., Han G.R., Enhanced Ferromagnetic Properties of Multiferroic $BiCo_xFe_{1-x}O_3$ Synthesized by Hydrothermal Method, *Materials Letters*, **62(23)**: 3806-3808 (2008).

[47] Wang S., "Preparation Process Analysis and Catalytic CO and NO Elimination Performance of LaCoO₃ Perovskite", M.S. Diss., Shenyang Normal University (2019).

[48] Gao X., "Study on Synthesis and Properties of Perovskite-Type LaCoO₃ Nanotubes", M.S. Diss., Tianjing University (2012).

[49] Wang S., Li Q., Gu W.X., Song Q.J., Teng Y., Preparation and Photocatalytic Properties of AgI-BiOCl Composites, *Applied chemical industry,* **50(353)**: 1751-1756 (2021).

[50] Li H.L., "Preparation of Perovskite Type Composite Metal Oxides and Study on Photocatalytic Reduction of CO_2 to Organic Esters", M.S. Diss., Tianjin University of Technology (2012).